

A Numerical Study of Brown Dwarf Formation via Encounters of Protostellar Disks

S. Shen,^{1*} J. Wadsley¹, T. Hayfield¹ and N. Ellens¹

¹ *Department of Physics and Astronomy, McMaster University, Main Street West, Hamilton L8S 4M1, Canada*

30 October 2018

ABSTRACT

The formation of brown dwarfs (BDs) due to the fragmentation of early-stage proto-stellar disks undergoing pairwise encounters was investigated. High resolution allowed the use of realistic, flared initial disk models where both the vertical structure and the local Jeans mass were resolved, preventing numerical enhancement or suppression of fragmentation. The results show that objects with masses ranging from giant planets to low mass stars can form during such encounters from disks that were stable before the encounter. The parameter space of initial spin-orbit orientations and the azimuthal angles for each disk was explored with a series of 48 simulations. For the types of interactions studied, an upper limit on the initial Toomre Q value of ~ 2 was found for fragmentation to occur. Depending on the initial configuration, shocks, tidal-tail structures and mass inflows were responsible for the condensation of disk gas into self-gravitating objects. In general, retrograde disks were more likely to fragment. It was also found that in fast encounters, where the interaction timescale was significantly shorter than the disks’ dynamical timescales, the proto-stellar disks tended to be truncated without forming objects.

The newly-formed objects had masses ranging from 0.9 to 127 M_J , with the majority in the BD regime. These often resided in star-BD multiples and in some cases also formed hierarchical orbiting systems. Most of them had large angular momenta and highly flattened, disk-like shapes. With the inclusion of the appropriate physics these could reasonably be expected evolve into proto-BD disks with jets and subsequent planet formation around the BD. The objects had radii ranging from 0.1 to 10 AU at the time of formation. The disk gas was assumed to be locally isothermal, appropriate for the short cooling times in extended proto-stellar disks but not for condensed objects. An additional case with explicit cooling that reduced to zero for optically thick gas was simulated to test the extremes of cooling effectiveness and it was still possible to form objects in this case. Detailed radiative transfer (not studied here) is expected to lengthen the internal evolution timescale for these objects so that they spend considerable time as puffed-up, prolate ellipsoids, but not to alter the basic result that proto-BD disks can form during proto-stellar encounters.

1 INTRODUCTION

Observations suggest that brown dwarfs (BDs, $0.013 M_\odot \lesssim m \lesssim 0.075 M_\odot$) are very abundant in both the field and star clusters in our galaxy (Chabrier 2002; Martín et al. 2001; Luhman 2000). The origin of brown dwarfs, however, is still under debate. It has been suggested by several authors (e.g., Whitworth et al. 2007; Bate et al. 2002) that the final stellar mass may be closely related to the Jeans mass of the parent gas within the molecular cloud. Given that the typical Jeans mass in a typical molecular cloud is of order one solar mass, this is reasonable for larger, hydrogen-burning stars. However, because BD masses are at least an order of magnitude smaller, it is difficult for BDs to form by direct collapse to pre-BD cores. Several scenarios have been proposed to circumvent this problem.

One approach is to assume that the initial Jeans mass of the core is still a good estimate of the final mass from a direct collapse, but that denser or colder regions exist where the Jeans mass may approach the BD mass. For example, Padoan & Nordlund (2004) proposed that local density of in cores can be enhanced by turbulent flows (“turbulent fragmentation”), while Elmegreen (1999) suggested that certain types of molecular cooling can greatly decrease core temperatures. In either case, formation of BDs follows the conventional star formation path. Hence, all properties associated with proto-stars, such as accretion disks and outflows, are expected.

An alternative picture, first proposed by Reipurth & Clarke (2001), suggests that the because the Jeans mass continuously decreases during the collapse,

arXiv:0909.2044v1 [astro-ph.SR] 11 Sep 2009

fragmentation can keep occurring repeatedly to produce smaller and denser objects until they are too dense to have efficient radiative cooling. The mass at this “opacity limit” is expected to be around $m_{\text{opacity}} \sim M_{\text{Jupiter}}$. Thus the opacity limit mass, rather than the initial core Jeans mass, would set the mass of the smallest fragments. In this scenario, it is normally assumed that these small masses form first. These so-called embryos then accrete mass and ultimately form both sub-stellar and stellar objects in a scenario referred to as “competitive accretion”. The accretion of the surrounding material onto embryos is assumed to be rapid so that embryos remaining in dense parts of the molecular cloud would ultimately become stellar-mass objects. Bate et al. (2003) explored this scenario with a simulation of cluster formation from a $50 M_{\odot}$ molecular cloud and found embryos could remain in the cloud undergoing rapid accretion or get ejected during violent interactions, resulting in a large number of low mass objects. More recent work indicates that a more realistic treatment of radiative energy losses can strongly suppress the formation of sub-stellar objects in such simulations (Price & Bate 2009).

The existence of extended disks around young stellar objects is supported by both observations and theory (e.g. Yorke & Bodenheimer 1999). The disks are initially large and flared at the class 0-I stage (extending to several thousands AU (see, e.g., Mundy et al. 2000) and are observable at mm or sub-mm wavelengths. They evolve into smaller, thin proto-planetary disks at the class III stage that are detectable with infrared observations. Disk lifetimes are inferred to be about 10 Myr. Disks provide a natural environment for forming sub-stellar objects because the Jeans mass in disks is much smaller than in cores. It may be possible to form brown dwarf mass companions through the fragmentation of marginally stable ($Q \sim 1$), extended disks around single stars (e.g., Stamatellos & Whitworth 2009). Whether disks become cold and heavy enough to spontaneously fragment depends on the disk mass build up from the envelope and the processes that are driving accretion. Self-regulated, stable ($Q > 1.5$), extended disks are the outcome for a significant portion of the parameter space (Vorobyov & Basu 2009).

The approach that will be investigated in this paper is encounter-triggered fragmentation of otherwise stable proto-stellar disks. Numerical studies by Watkins et al. (1998a,b) and Lin et al. (1998) have independently found that instabilities leading to bound companions can be triggered during encounters between stable proto-stellar disks. Fragmentation was seen to occur within the disk (Watkins et al. 1998b), or in filamentary structures induced by the tidal force between the encountering disks (Lin et al. 1998). The resultant objects reported by both groups include sub-stellar mass objects.

Since most stars form in clusters with a relatively small spread in ages (Gauvin & Strom 1992), it is reasonably likely that a proto-star will undergo an encounter during the time that the disks are large (e.g. Thies et al. 2005; Watkins et al. 1998a). Following the argument by Thies et al. (2005), for a Plummer star cluster model with mass of $500 M_{\odot}$ and a half-mass radius, $R_{0.5} = 0.5$ pc, the encounter probability in 5×10^5 years (the approximate lifetime for an early extended disk) with an impact param-

eter at pericenter of 500 AU is about 30 percent. If several sub-stellar objects form during each encounter, as in Watkins et al. (1998a), a substantial numbers of BDs can be produced. In this work, we focus on the outcomes of specific encounters rather than estimates of their likelihood.

The prior simulation work failed to address several important issues. Firstly, the resolution used in the work cited above did not ensure that the Jeans mass was resolved in the original disks. Thus it was not clear whether the objects might have condensed due to numerical effects (Bate & Burkert 1997; Truelove et al. 1997).

Secondly, the range of circumstances in which gravitational instabilities can be triggered in a stable disk by an encounter were not explored. The Toomre criterion for instability requires that that $Q < Q_{\text{crit}}$ for thin disks to be unstable to axisymmetric perturbations, where Q is the Toomre parameter, locally defined according to (Toomre 1964),

$$Q \equiv \frac{c_s \kappa}{\pi G \Sigma}, \quad (1)$$

where c_s is the sound speed, κ is the epicyclic frequency (close to the angular speed Ω for a Keplerian disk) and Σ is the disk surface density. Analytical studies by Toomre (1964) and numerical studies of relatively thin proto-planetary disks (Boss 2001; Mayer et al. 2004; Pickett et al. 2003; Gammie 2001) have shown that Q_{crit} is in the range 1-1.5 for various modes of fragmentation. If proto-stellar disks are stable according to this criterion then they tend to stay so indefinitely in the absence of mechanisms to redistribute material. A non-negligible (vertical) thickness for the disks can be stabilizing, reducing the critical Q value for axisymmetric perturbations from 1 down to 0.6 – 0.7 (Kim et al. 2002). The evolution of the Toomre parameter during dynamical interactions is a good indicator for the onset of instabilities and fragmentation and this has been explored here. It should also be noted that the initial disk models assumed in prior work did not resolve the disk vertical structure, which can destabilize the disk (by increasing the effective critical Toomre Q) and artificially enhance fragmentation. These issues motivated our use of detailed, vertically-resolved initial disk models.

Lastly, there have been few predictions regarding the properties of the young BDs that could be produced during a proto-stellar disk encounter. Most observed young brown dwarfs show signatures of surrounding disks analogous to the disks around proto-stars, and some of these disks have been identified as accretors through spectral line analysis (e.g. Jayawardhana et al. 2003). The detection of BD accretion disks has been used as an evidence to support the turbulent fragmentation scenario (see, e.g. Padoan & Nordlund 2004) against dynamical formation mechanisms, especially after the aforementioned simulation by Bate et al. (2003) produced an practically no proto-BD disks. Early encounter simulations, such as the ones by Lin et al. (1998) and Watkins et al. (1998a,b), also reported no proto-BD disks. However, these negative results are quite likely to reflect insufficient resolution or the impact of approximations such as replacing the fragments with a large “sink” particles (Bate et al. 2003). Studies with better resolved disks and fragments were thus required to address this question.

The current study investigated encounter-induced BD formation using a series of high resolution hydrodynamical

cal simulations. This allowed the Jeans mass to be resolved until well after fragmentation initially took place and the vertical structure of the initial disks was also well resolved. The paper is organized as follows: in section 2 we describe the numerical method, the construction of the initial disk models and a study of resolution requirements. In section 3 we present the encounter parameter space being explored, including Q values, relative orientations of disks and variations in encounter velocity. Section 4 describes several typical simulations and discusses the conditions for encounter-induced fragmentation. Section 5 presents analysis of the properties of the resultant objects, including shapes, angular momenta and orbital evolution. Section 7 summarizes the results and includes discussion of the observational implications and possible directions for future work.

2 METHODS

2.1 Proto-Stellar Disk Model

Observing the exact mass, density structure and kinematics of proto-stellar objects during the earliest stages is difficult (White et al. 2007). Using a hydrodynamical calculation of proto-stellar disk formation, Yorke & Bodenheimer (1999) found that early disks contain a large fraction of the total mass of the system and collapse relatively slowly. Based on these results, we assumed that the proto-stellar disks were quasi-hydrostatic in order to construct a self-consistent disk density structure.

We chose to simulate systems in the solar mass range with a single model for the disk-*proto-star* system where the disk mass was about $0.6 M_{\odot}$, with a stellar mass of around $0.5 M_{\odot}$. The disk extended to about 1000 AU. This aspect of the set-up is similar to the disks simulated by Watkins et al. (1998a,b). A power-law surface density profile $\Sigma = \Sigma_0^{-p}$ was chosen with $p = 1.5$ in 100-500 AU, consistent with observations of early proto-stellar disks (Andre et al. 2000). The surface density peaked at 100 AU with $\Sigma_{max} \sim 20.0 \text{ g/cm}^3$. Within 100 AU the gas was initially smoothly truncated. We relaxed our initial disks in isolation for about 10000 years, during which a small amount of material occupied the truncated region. Beyond 500 AU the surface density falls rapidly but smoothly, and at 1000 AU $\Sigma \sim 0.03 \text{ g/cm}^3$. The entire profile after relaxation is similar to the results from core collapse calculations by Yorke & Bodenheimer (1999). Most of the disk mass ($0.5 M_{\odot}$) is within 500 AU.

It was assumed that the central *proto-star* was the major heating source for the disk, and that the disk radiates like a black-body, giving a disk temperature profile of $T(r) \propto r^{-1/2}$ (Mayer et al. 2004; Pickett et al. 2003; Chiang & Goldreich 1997) for the majority of the simulations. The profile smoothly transitions to an external, ambient temperature of $\sim 40 - 80 \text{ K}$. This profile is similar to the Yorke & Bodenheimer (1999) results. With the radial surface density and temperature profiles specified, the vertical structure was iterated to a self-consistent hydrostatic equilibrium taking into account both the gravity of the central star and the self-gravity of the disk. Accurate treatment of the gas self-gravity was important given the large disk mass relative to the star.

2.2 Radial Toomre Q Profile

The choice of radial profile gave a nearly constant Q value between 100-500 AU, with a minimum value (Q_{min}) ranging from 1.6 to 2.1 depending on the case studied. The Q value rises in the inner 100 AU and the disk is very stable there. Test simulations of single disk evolution with different values of Q_{min} were performed, and it was found that for our disk model values of Q_{min} below $Q_{crit} = 0.8$ were required for spontaneous fragmentation via spiral waves. This critical value was lower than the ones seen in thin disk models (e.g., $Q_{crit} = 1.4$ in Mayer et al. (2004)), consistent with the results from Kim et al. (2002) that significant scale heights tend stabilize the disk. To rule out spontaneous fragmentation as a factor during the dynamical interactions between disks, the Q_{min} values used were at least twice as the Q_{crit} for an isolated disk, i.e. $Q_{min} \geq 1.6$.

2.3 Heating and Cooling Approximations

A fixed temperature profile $T(r) \propto r^{-1/2}$ for most of the disk was used in the majority of our simulations, which is often referred to as a locally isothermal equation of state (EOS). Heating sources other than the star, such as shocks, were not taken into account. For the current study, it was found that the isothermal EOS was a good approximation for the initial disk and also acceptable even after disk was heated by tidal structures and shocks (outside the clumps) because the disks are extended and initially optically thin. Given the temperature of the gas, using the surface density profile described above and adopting the opacities from D'Alessio et al. (2001), the product of the disk cooling time t_{cool} and angular rotation rate Ω was calculated and $\Omega t_{cool} = 0.3 - 0.7$ beyond 50 AU for the initial disk, which is comfortably within the cooling requirement for the disk to fragment $\Omega t_{cool} < 12$ (Rice et al. 2005; Johnson & Gammie 2003) before the disk is dense enough for the isothermal assumption breaks down. However, after the disk fragments and the resultant objects became gravitationally bound, the final densities of these objects were typically orders of magnitude larger than the initial values and the objects were thus optically thick. Thus our locally isothermal approximation was initially good but later became an upper bound on how efficient cooling should be. To further examine the importance of cooling in fragmentation, a case was also investigated with explicit cooling that became negligible in the optically thick regime. This second assumption is a lower bound for the cooling in a real disk as it disallows even the slow leakage of radiation from dense gas. The results of this case are described in section 6.

2.4 Simulations

We used the TreeSPH code GASOLINE (Wadsley et al. 2004) to model the disks during encounters. Around 200,000 particles were used for each $0.6 M_{\odot}$ disk, with each particle representing ~ 1 Earth mass. This resolution was chosen to satisfy the condition that the local Jeans mass should be resolved by at least $2N_{neighbor}$ (Bate & Burkert 1997) to prevent numerical fragmentation, where $N_{neighbor}$ is the number of neighbor particles in SPH (Smoothed Particle Hydrodynamics) simulation. The number of particles ensured

that the Jeans mass was not-only well resolved in the initial condition, but also well-resolved when density was enhanced during an encounter (when the Jeans mass decreased), up to a density $\rho \sim 10^{-10} \text{ g cm}^{-3}$ (about 10^3 times the initial maximum value in the disk). Resolving the Jeans mass within the fragments, however, was not attempted due to high computing costs ($N > 10^7$ particles usually required). Therefore, our choice of particle numbers ensures physically correct modeling of the initial fragmentation in the protostellar disk, but cannot ensure that any secondary fragmentation of the clumps themselves are physical.

The initial disk model also resolved the scale height at the mid-plane very well at 100 AU (where the local smoothing length was about 1.9 AU and the scale height was about 6 AU). Within 50 AU the scale height of the disk was less well resolved and the orbital time was shortest so that artificial viscous evolution could have been a concern. The artificial viscosity was moderated using the Balsara switch which helps to suppress unwanted shear effects. The measured viscous time scale in the code was about 10^8 to 10^{11} years, much longer than the dynamical scale of the encounter, $t \sim 10^5$ years. Hence, the effect due to the viscous evolution was negligible. Appendix A presents an exploration of the effects of unresolved Jeans mass and unresolved disk scale height.

The gravitational softening, ϵ , for gas particles was 0.2 AU, one tenth of the smallest particle spacing in the initial condition. Thus dense regions up to 1000 times the initial densest part were well resolved. Since a larger ϵ usually suppresses gravitation forces, the choice of gravitational softening will tend to inhibit fragmentation once the particle separations are comparable to or smaller than the softening. In all tests, including those done for this work and in other work to date, there have been no indications that the Gasoline code suffers from artificial fragmentation as a consequence of the gravitational softening being smaller than the local SPH smoothing length. The fixed softenings ensure accurate gravitational dynamics at the cost of having somewhat conservative time steps in lower density regions.

The central proto-star was represented by a single 0.5 solar mass sink particle for which the softening was set to 1 AU. The sink acted within a 1 AU radius around the star to consume gas falling into the innermost regions and thus avoid the small time steps required for gas orbiting very close to the star. However, no objects formed during the simulation were replaced with sink particles, ensuring that any disks surrounding the newly formed, sub-stellar object were modeled directly.

3 PARAMETER SPACE

3.1 Locally Isothermal Simulations

In each pairwise disk encounter, the two disks were identical in size, mass and Toomre parameter with an initial impact parameter of 1000 AU. Due to gravitational focusing during relatively slow encounters the minimum distance between two stars could become substantially less than the initial impact parameter. The initial disk separation was 6000 AU. This system was initially bound if the relative velocity of the encounter is less than 0.8 km/s and the final impact parameter is a function of the relative velocity. This study explored six dimensions in the overall parameter space:

- (i) The initial Toomre parameter profile characterized using the minimum value, Q_{\min} ;
- (ii) The geometric configuration of the encounter, including the angles between the two disk planes and the angles between the disk planes and the plane of the orbit of the two disks (a total of four independent parameters);
- (iii) The relative velocity of the encounter.

Mass, disk size and impact parameter variations were not included to limit the study to a manageable size. Smaller impact parameters are possible but considerably less likely. These variations may be explored in future work.

A list of all the simulations is shown in Table 1. The first 3 cases (Q1, Q2, Q3) were carried out to study the effect of the Toomre parameter on encounter-triggered fragmentation with different initial minimum Q values of 1.6, 1.8 and 2.1, respectively. A higher Q profile means a more stable initial condition, for which more effort is required to trigger fragmentation. We selected an encounter configuration where fragmentation was likely (coplanar, retrograde disks) to first explore the threshold in initial Toomre Q_{\min} , above which dynamical interactions would become insufficient to trigger fragmentation. This study helped to constrain the region of interest within the parameter space.

Previous work by Lin et al. (1998) indicated that fragmentation can take place in tidal structures forming during encounters while Watkins et al. (1998a,b) suggested disks would fragment. The degree of tidal distortion and angular momentum transport has been shown to depend on the initial disk spin orientations (with respect to the orbital angular momentum) (Toomre & Toomre 1972). Various disk spin orientations were used in our simulations including prograde cases (where the angle between the angular momentum vector of the disks and that of the orbit was less than 90 degrees), retrograde cases (where the spin-orbit angle was greater than 90 degrees) and combinations of the two.

In most simulations the disks were not close to the same plane, as would be expected for randomly oriented disks. However, coplanar encounters (where the spin-orbit angles are zero) were also simulated as special cases to investigate the shocks generated in such encounters and the possibility of shock fragmentation. In every case the orbital plane was the x-y plane so that the orbital angular momentum was in the direction of the z-axis.

In a completely generic encounter, as shown in Figure 1, the disks can be oriented randomly. The configuration of each disk in the encounter can then be characterized by two angles: the angle between the spin angular momentum of each disk and the positive z direction, θ , and the angle between the positive x direction and the projection of disk angular momentum onto the x-y plane, ϕ , which also determines where that disk intersects the x-y plane. The initial disk velocities are always along the x-axis and the initial impact parameter is due to an offset in the y-direction.

Cases Conf1-48 explored the $(\theta_1, \phi_1, \theta_2, \phi_2)$ parameter space. For a single disk, the angle parameters were selected such that the θ space (from 0 to 180 degrees) was divided evenly into three ranges and the ϕ space (from 0 to 360 degrees) into four for a total of 12 cases. Naively there would have been 144 possible combinations of disks but due to the symmetry of the encounters and the equivalence when the two disks were exchanged in space, there were 42 unique

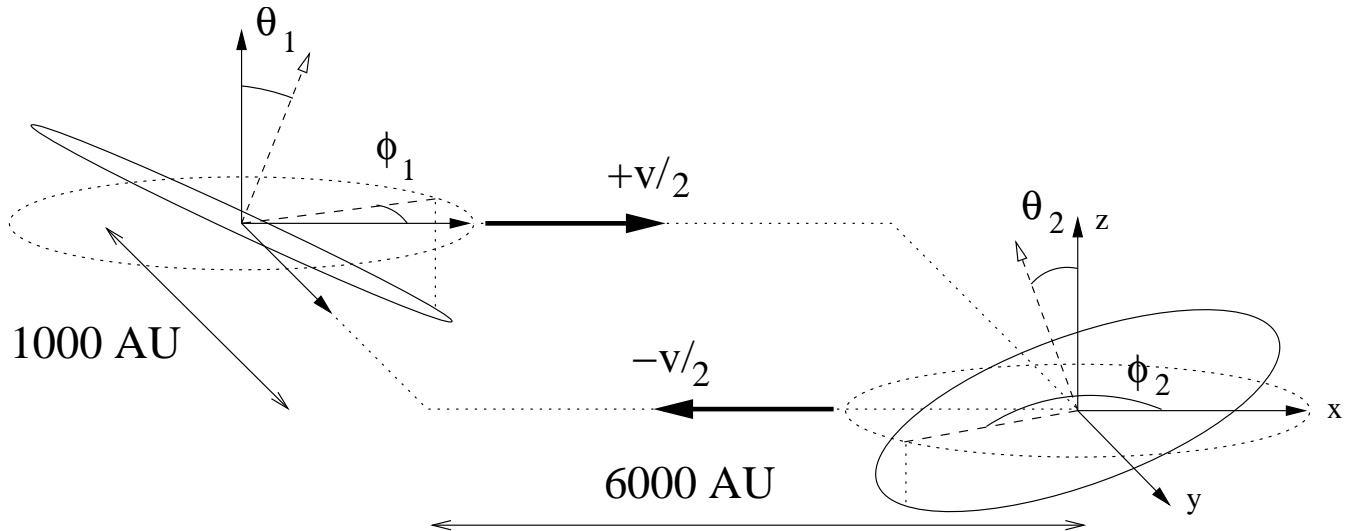


Figure 1. A generic encounter configuration between two proto-stellar disks. The centres of mass orbit in the x-y plane with an initial velocity solely in x-direction. The angular momentum of an individual disk has a vector direction that differs from the orbital angular momentum (the z-axis) by an angle θ . The disk angular momentum vector projected onto the x-y plane makes an angle ϕ with the x-axis.

collisions to simulate. An additional six cases were simulated where at least one disk was exactly in the orbital plane, to investigate the effects of coplanar encounters.

The cases with labels starting with “Vel” refer to two series of runs used to examine the constraints due to the initial relative velocity on disk fragmentation for prograde and retrograde encounters. Relative encounter velocities in the range of 0.8 km s^{-1} to 6.0 km s^{-1} were used in the simulations to investigate the effects of relative velocity on disk fragmentation. The inferred disk velocities are consistent with the typical velocity dispersion in stellar clusters (a few km s^{-1} , See e.g., Bate et al. 2003, and references therein)

4 NUMERICAL RESULTS OF THE PARAMETER SPACE STUDY

4.1 Varying Toomre Q parameters

To explore the impact of the initial minimum Toomre parameter we investigated 3 cases, all of which have $(\theta, \phi) = (180, 0)$ and relative $v = 0.8 \text{ km/s}$. These systems are only marginally unbound. These collision parameters were chosen to ensure a strong interaction (detailed discussion in Section 4.2) so that if no fragments form in these calculations then they are also not likely under other configurations and encounter speeds. The two disk are coplanar since they have the same θ and ϕ .

Case “Q1” ($Q_{\min}=1.6$) is depicted in Figure 2. When the physical impact began, the gas was shock compressed and quickly formed a “shock layer” between the two disks where the density was substantially enhanced. At 24,000 years after the encounter, the shock fragmented to form a $7 M_J$ clump at about 223 AU away from the nearest star (label “a” in Panel 5, Panel 7). Also, due to its retrograde configuration, the angular momentum of the disk spin and the orbit are opposed and thus the rotation speed of the gas decreases. As a result, a large amount of gas spirals into the inner disk (within $\sim 100 \text{ AU}$ in this case), while gas in

the outer disk dissipates. The azimuthally averaged surface density profile of the lower-left disk in Panel 4 of Figure 2 is shown at different times in Figure 3 and the corresponding evolution of azimuthally averaged Q profile is shown in Figure 4. At $t = 23,000$ years, the surface density had increased significantly, and at $r \sim 10 - 20 \text{ AU}$, it had almost doubled its value from earlier times ($t = 6,000$ years, well before the physical impact of gas materials). However, Q was still very high in the inner 100 AU because of the fixed high temperature in that region (Figure 4). Thus it was the presence of the shock layer at around 200 AU that locally increased the surface density and lowered the Toomre Q down to unity ($Q_{\min} = 1$, Figure 4) allowing a strong spiral feature to form which is gravitationally unstable. At $t = 24,000$ years, a pair of close clumps formed at $r \sim 130 \text{ AU}$ with masses of about 12 and 14 M_J (labeled “b” in Panel 5, Panel 8), and at about 150 AU another gas blob started condensing (a moderate extremum near the 130 AU clump in the plot of the Q profiles, labeled “c” in Panel 5), which eventually became a bound object (labeled “d” in Panel 6). Gas inflow increased after formation of these objects. At $t = 24,400$ years, fragmentation within 20 AU was finally triggered in one of the disks and 4 brown-dwarf mass clumps were formed (boxed region in Panel 6, Panel 9). However, these objects were not included in our statistics (Section 5) because the density within 20 AU at this time step exceeded $10^{-12} \text{ g cm}^{-3}$ and became optically thick (cf. Section 6), so that an isothermal cooling assumption was no longer appropriate. The simulation was stopped at $t = 24,400$ years because the time step reduced dramatically after the first condensation formed. Analysis based on the energy and momentum at the end of simulation indicates that amongst the 4 objects formed outside 100 AU, one is unbound and likely to leave the system, one has a large semi-major axis ($a = 879.3 \text{ AU}$) and the other two have orbits with semi-major axes less than 100 AU.

The encounter “Q2” has same parameters as “Q1” except the initial $Q_{\min} = 1.8$. The disk underwent similar

Table 1. Simulation Parameters

Case	Toomre Q_{\min}	(θ_1, ϕ_1) (deg)	(θ_2, ϕ_2) (deg)	v (km/s)	N_1	N_2
Q1 (Vel_retro1)	1.6	(180, 0)	(180, 0)	0.8	3 (1)	0 (4)
Q2	1.8	(180, 0)	(180, 0)	0.8	0	0 (1)
Q3	2.1	(180, 0)	(180, 0)	0.8	0	0
Conf1	1.6	(180, 0)	(180, 0)	2.0	0 (1)	0 (1)
Conf2	1.6	(0, 0)	(0, 0)	2.0	3	4
Conf3 (Vel_pro2)	1.6	(0, 0)	(45, 0)	2.0	1	2
Conf4	1.6	(180, 0)	(135, 0)	2.0	1	0 (1)
Conf5	1.6	(180, 0)	(45, 0)	2.0	2 (1)	0
Conf6	1.6	(150, 110)	(150, 110)	2.0	1 (1)	2 (1)
Conf7	1.6	(150, 110)	(150, 250)	2.0	0	4
Conf8	1.6	(150, 110)	(150, 290)	2.0	0	3 (1)
Conf9	1.6	(150, 70)	(150, 70)	2.0	2	3
Conf10	1.6	(150, 70)	(150, 110)	2.0	0	3 (1)
Conf11	1.6	(150, 70)	(150, 250)	2.0	4	3 (1)
Conf12	1.6	(150, 70)	(150, 290)	2.0	1 (1)	2 (1)
Conf13	1.6	(30, 110)	(150, 110)	2.0	0	9 (1)
Conf14	1.6	(30, 110)	(150, 250)	2.0	1 (1)	0 (1)
Conf15	1.6	(30, 110)	(150, 290)	2.0	0	5 (1)
Conf16	1.6	(30, 70)	(150, 70)	2.0	0	3 (2)
Conf17	1.6	(30, 70)	(150, 110)	2.0	0	6 (1)
Conf18	1.6	(30, 70)	(150, 250)	2.0	0	0
Conf19	1.6	(30, 70)	(150, 290)	2.0	0	3 (2)
Conf20	1.6	(30, 110)	(30, 110)	2.0	3 (1)	0
Conf21	1.6	(30, 110)	(30, 250)	2.0	0	0
Conf22	1.6	(30, 110)	(30, 290)	2.0	3	2
Conf23	1.6	(30, 70)	(30, 70)	2.0	1 (1)	1 (1)
Conf24	1.6	(30, 70)	(30, 110)	2.0	0	0
Conf25	1.6	(30, 70)	(30, 250)	2.0	0	3
Conf26	1.6	(30, 70)	(30, 290)	2.0	1	0
Conf27	1.6	(30, 110)	(90, 135)	2.0	0	2
Conf28	1.6	(30, 110)	(90, 225)	2.0	0	1 (1)
Conf29	1.6	(30, 110)	(90, 315)	2.0	0	0
Conf30	1.6	(30, 70)	(90, 45)	2.0	0	3 (1)
Conf31	1.6	(30, 70)	(90, 135)	2.0	0	5
Conf32	1.6	(30, 70)	(90, 225)	2.0	0	1
Conf33	1.6	(30, 70)	(90, 315)	2.0	0	3
Conf34	1.6	(90, 135)	(150, 110)	2.0	0	4 (5)
Conf35	1.6	(90, 135)	(150, 250)	2.0	5 (1)	5
Conf36	1.6	(90, 135)	(150, 290)	2.0	3 (3)	0
Conf37	1.6	(90, 45)	(150, 70)	2.0	0	2 (1)
Conf38	1.6	(90, 45)	(150, 110)	2.0	2	3
Conf39	1.6	(90, 45)	(150, 250)	2.0	4 (1)	0
Conf40	1.6	(90, 45)	(150, 290)	2.0	0	5
Conf41	1.6	(90, 135)	(90, 135)	2.0	0	0
Conf42	1.6	(90, 135)	(90, 225)	2.0	2 (1)	0
Conf43	1.6	(90, 135)	(90, 315)	2.0	0	0
Conf44	1.6	(90, 45)	(90, 45)	2.0	0	0
Conf45	1.6	(90, 45)	(90, 135)	2.0	0	0
Conf46	1.6	(90, 45)	(90, 225)	2.0	0	0
Conf47	1.6	(90, 45)	(90, 315)	2.0	1	4
Conf48	1.6	(0, 0)	(90, 0)	2.0	0	3 (1)
Vel_pro1	1.6	(0, 0)	(45, 0)	0.8	0 (1)	0
Vel_pro2(Conf3)	1.6	(0, 0)	(45, 0)	2.0	1	2
Vel_pro3	1.6	(0, 0)	(45, 0)	4.0	0	0
Vel_pro4	1.6	(0, 0)	(45, 0)	6.0	0	0
Vel_retro1(Q1)	1.6	(180, 0)	(180, 0)	0.8	3 (1)	0 (4)
Vel_retro2	1.6	(180, 0)	(180, 0)	2.0	0 (1)	0 (1)
Vel_retro3	1.6	(180, 0)	(180, 0)	4.0	1 (1)	0
Vel_retro4	1.6	(180, 0)	(180, 0)	6.0	0	0

The pairs (θ_1, ϕ_1) and (θ_2, ϕ_2) denote the angles between the disk angular momentum vector and the angular momentum vector of the orbit and the angular momentum vector and the vector direction of the initial velocity difference in the orbital plane for disk 1 and disk 2 respectively. v denotes the relative encounter velocity. The number of objects formed for each disk are shown in the last two columns. If objects were formed within 50 AU then the

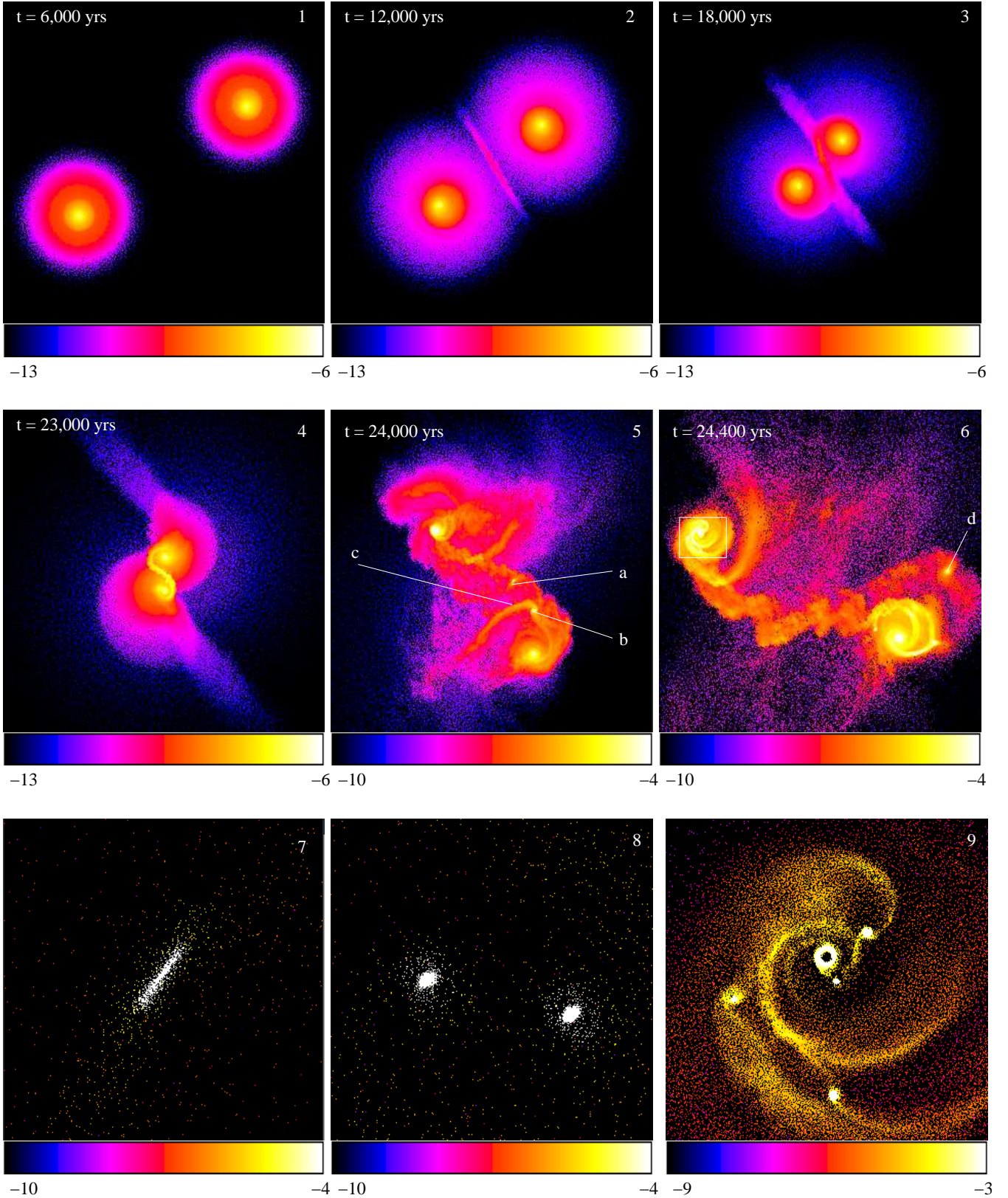


Figure 2. A coplanar encounter between two retrograde disks with $Q_{min} = 1.6$. Panels 1 to 6 are snapshots of the simulation, with the time indicated at the left top of each panel. The disk were rotating clockwise in all of the panels. The color bar under each panel gives the logarithm (base 10) of the density in units of M_{\odot}/AU^3 . In panels 4 and 5 only the inner dense regions were included and a different density range was used as indicated. Panels 7 and 8 are zoomed-in pictures of objects formed from a shock layer and due to disk fragmentation (a and b in panel 5), respectively. Panel 9 is the zoomed-in picture of the boxed region in panel 6, showing fragmentation of the inner disk.

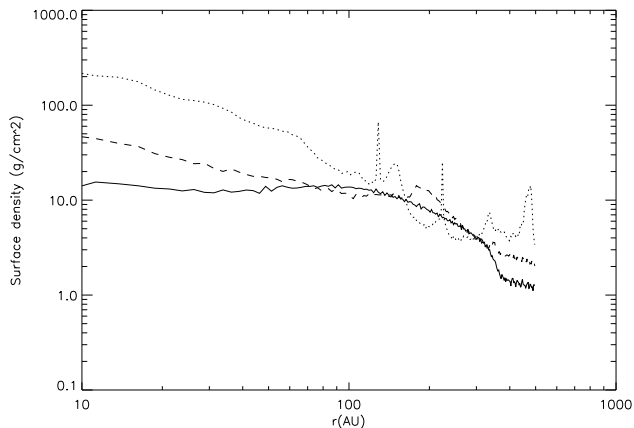


Figure 3. Evolution of the surface density profile for the case in Figure 2. *Solid line:* Surface density profile of one of the encountering disks at 6,000 years. *Dashed line:* Surface density profile for the same disk at 23,000 years. *Dotted line:* Surface density profile at 24,000 years. The sharp peak at 130 AU is produced by two close objects forming due to disk fragmentation, the one at 225 AU originates from shock layer fragmentation. The moderate peak in between indicates ongoing gas condensation.

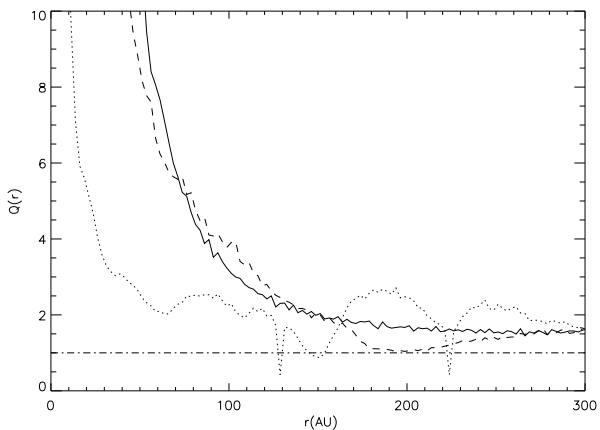


Figure 4. The Toomre Q profile for the same disk as in Figure 3 at 6,000, 23,000 and 24,000 years (solid, dashed, dotted line, respectively). The dot-dashed line indicated $Q = 1.0$

physical processes such as formation of a layer of shock-compressed gas, inflow of gas and disk truncation after the encounter. Nevertheless, the disks were more stable to the perturbation and only one of the disks developed an $m = 2$ mode gravitational instability at a relatively late time step ($t = 25,300$ years), which then fragmented and formed only one bound object at radius of 30 AU. The other disk was truncated but remained stable. The gas in the shock layer did not condense to form an object. Instead, it dispersed after the disks moved apart. The lowest Q value at $t = 24600$ years (the time step just before fragmentation) for the unstable disk was 1.1 and for the stable disk was 1.7, close to the original minimum.

The last case in this series “Q3” used initial disks with $Q_{\min} = 2.1$. The encounter disrupted both disks without forming any objects. The two stars happened to capture each

other and formed a close binary system with a separation of about 20 AU. Most of gas was dispersed, with the bound gas at the end of simulation forming a circumbinary disk with a radius of 250 AU at 31000 years. The circumbinary disk had a much lower surface density compared to the initial disks. Assuming the gas was still in Keplerian rotation, the minimum Toomre Q was very high ($Q_{\min} = 6.2$). The disk was thus very stable against spontaneous fragmentation and no clumps were expected to form in future evolution.

The cases described here showed that instability and fragmentation can be triggered in an initially stable disk by pairwise encounters. However, the initial minimum Toomre parameter can not be higher than 2.1 for instabilities to occur. From the evolution of the Q profile in Figure 4 it can be seen that lowering Q down to unity is crucial for fragmentation. Two competing processes, gas inflow and dispersion, proceed at the same time in an encountering disk. In a high Q disk the gas is hotter and an encounter is more likely to accelerate the gas dispersion rather than triggering gas inflow as in the relatively low Q (but still initially stable) cases. Indications are that early stage proto-stellar disks are usually large, heavy and relatively cold, with temperatures not far from those of the molecular cloud core ($\sim 10K$). So gas inflow can be the key mechanism in encounter-induced disk fragmentation.

Note that the local enhancement of density in the shocked gas can lower the Q parameter significantly and induce disk instability before the inflowing gas reduces Q in the inner, hotter region, making the fragments form relatively far from the stars. This is especially clear for coplanar encounters discussed in this section. In more likely, non-coplanar cases (cf. Section 4.2) the shocked gas usually does not form a well-defined layer between the disks, but it remains an important factor driving disk instability. In the case “Q1” the shock layer itself also fragmented directly. The object formed this way was not associated with spiral structure in the unstable disk (panel 5 in Figure 2). Fragmentation of shock layers rarely occurs and was restricted to coplanar, low-velocity, low- Q cases. With higher disk temperature (as in “Q2”) or higher velocity the shock layer usually dissipates when the two stars pass periastron without forming objects.

4.2 Varying the Encounter Configurations

The parameter space of encounter configurations was explored with 48 encounters covering the (θ, ϕ) parameter space. The effect of the relation between disks’ spin and orbital angular momentum in z direction can be seen by varying the disks’ θ parameters. This variation qualitatively changes the interactions, including the mechanisms of fragmentation.

There is a large stochastic element to the evolution of the disks and the formation of clumps. In this sense, the precise number of objects formed in a single simulation should not be examined too closely. For example, a small perturbation in the initial particle placements that is within the noise in the initial surface density profile is sufficient to change the outcome in terms of the precise number and placements of clumps. For example, several cases are symmetric from the point of view of the two disks but have non-symmetric outcomes. Symmetry in the configurations is revealed by the mappings $x, y, z \rightarrow -x, -y, z$ which implies $\theta_1 = \theta_2$ and

$\phi_1 = \phi_2$ (such as for the coplanar cases and “Conf6”, for example) and $x, y, z \rightarrow -x, -y, z$ which gives $\theta_1 = \theta_2$ and $\phi_1 = \phi_2 + 180$ (e.g. “Conf11”). These initial states were created using absolute offsets ($x \rightarrow x + \Delta x$) of two identical disks that have small non-axisymmetric perturbations due to the glass initial particle state. Thus the small perturbations in the particle configurations are not symmetric in these cases. These difference magnify during the course of the encounter and ultimately result in different numbers of objects in each disk as can be seen in the object numbers for each disk in symmetric cases in table 1. For example disk 1 in “Conf6” made 2 objects while Disk 2 made 3. The variations are consistent with a Poisson-type random process. In most of our analyses we look at outcomes averaged over several encounters.

4.2.1 Formation of Tidal Structures in Prograde Disks and Fragmentation

Encounters between retrograde disks tended to reduce the disk spins and cause gas inflows, increasing the surface density of the inner disks and reducing the Toomre Q parameter (Figure 2). Prograde encounters are more complex as seen in Figure 5 showing snapshots of encounter “Conf3”. The two disks have $(\theta, \phi) = (0, 0)$ and $(45, 0)$, respectively. The encounter had a relative speed 2.0 km/s and the initial minimum Q of the disks was 1.6. Gas between the two disks was shock-compressed (Panel 2 in Figure 5), though it did not form a layer or fragment. In prograde cases spin-orbit resonances can occur. Gas in the resonance region is continuously perturbed promoting angular momentum transport that simultaneously enhances the density of the inner disk while the outward gas flows collect a substantial portion of the disk mass into filamentary tidal structures (Figure 5, Panel 4), analogous to the tidal tail structures generated during the interaction between two prograde disk galaxies. In the case shown, at 14,000 years gas began condensing from a tidal structure of one disk (on the right in Panel 4) at about 320 AU from the star (labeled “a” in Panel 4), which later formed a bound object of mass $\sim 20 M_J$. A tidal structure was also present in the other disk, where there was a 45 degree angle between the spin and orbital angular momentum vectors. At 15,000 years, it condensed into two objects with masses of $9 M_J$ and $70 M_J$ at 60 and 110 AU from the star, respectively (labeled “b” in Panel 5 Figure 5). The simulation was terminated at 16,000 years. Analysis based on the energy and momentum of the objects found that all the 3 objects remained bound to the system but their orbits were large: 532 AU for the one that condensed first, and 90 and 307 AU for the two condensed in the later time step.

Fragmentation of tidal structures was seen in several prograde disk encounters, especially when the disk was closely aligned with the orbital plane. This result is consistent with Lin et al. (1998), in which a disk-disk encounter triggered formation of a large tidal tail and an object condensed from it. Objects formed this way tend to have large orbital radii. For example, in the case “Conf2”, tidal structures from both disks condensed and formed 7 objects in total by the end of simulation, all of which were unbound to both stars.

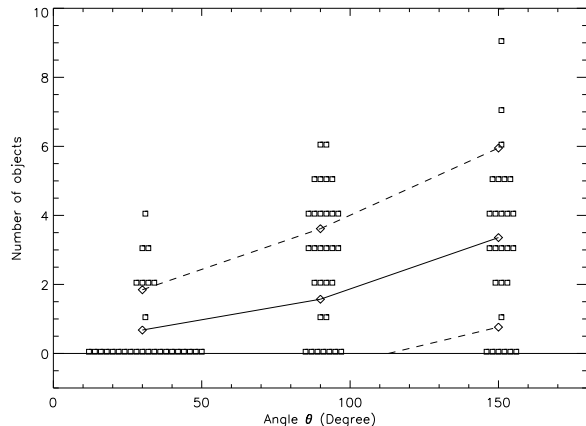


Figure 6. The number of objects formed in a disk per encounter as a function of θ . Each box corresponds to a single simulated disk that produced the number of objects indicated on the y-axis. The boxes have been spaced apart in the x-direction for clarity. The average and variance are indicated with solid and dashed lines respectively.

4.2.2 Prograde vs. Retrograde Encounters

Tidal structures due to spin-orbit resonances are not as efficient at producing objects as the inner disk fragmentation seen in retrograde disks. On the other hand, Watkins et al. (1998a) has argued that star formation triggered by collisions of molecular clouds tends to result in prograde-prograde coplanar encounters so they may be more common.

In Figure 6 we plot the number of object formed in a disk per encounter as a function of θ , the angle between the individual disk spin vector and the positive z direction. We chose the homogeneous sample from “Conf6” to “Conf48” in Table 1, excluding the unlikely coplanar encounters, $\phi = 0$ encounters and encounters with disks residing in the orbit plane. The cases chosen all have same initial Toomre parameter and relative encounter speed.

The average number of bound and unbound objects formed within that disk increases with increasing θ for that disk. This is the case regardless of the configuration of the other disk in the interaction. Gas inflow efficiently adds mass to inner disks which fragment whereas in prograde disks, the mass transfer usually send substantial amounts of gas outward rather than inward. The condensation of tidal structures did not occur frequently, because in most of the cases they usually dissipated before anything could form.

4.2.3 Plane-Parallel Encounters

No clear correlation was found between the productivity of a disk and the disk’s own ϕ parameter. However, no fragmentation would happen if the two disk planes are parallel (or nearly parallel) initially but not coplanar. 60% of the encounters in the “Conf” series which do not produce any clumps fall into this category. The disks were simply truncated in these cases. The final size of the disk is about 300 to 500 AU depending on the initial configuration.

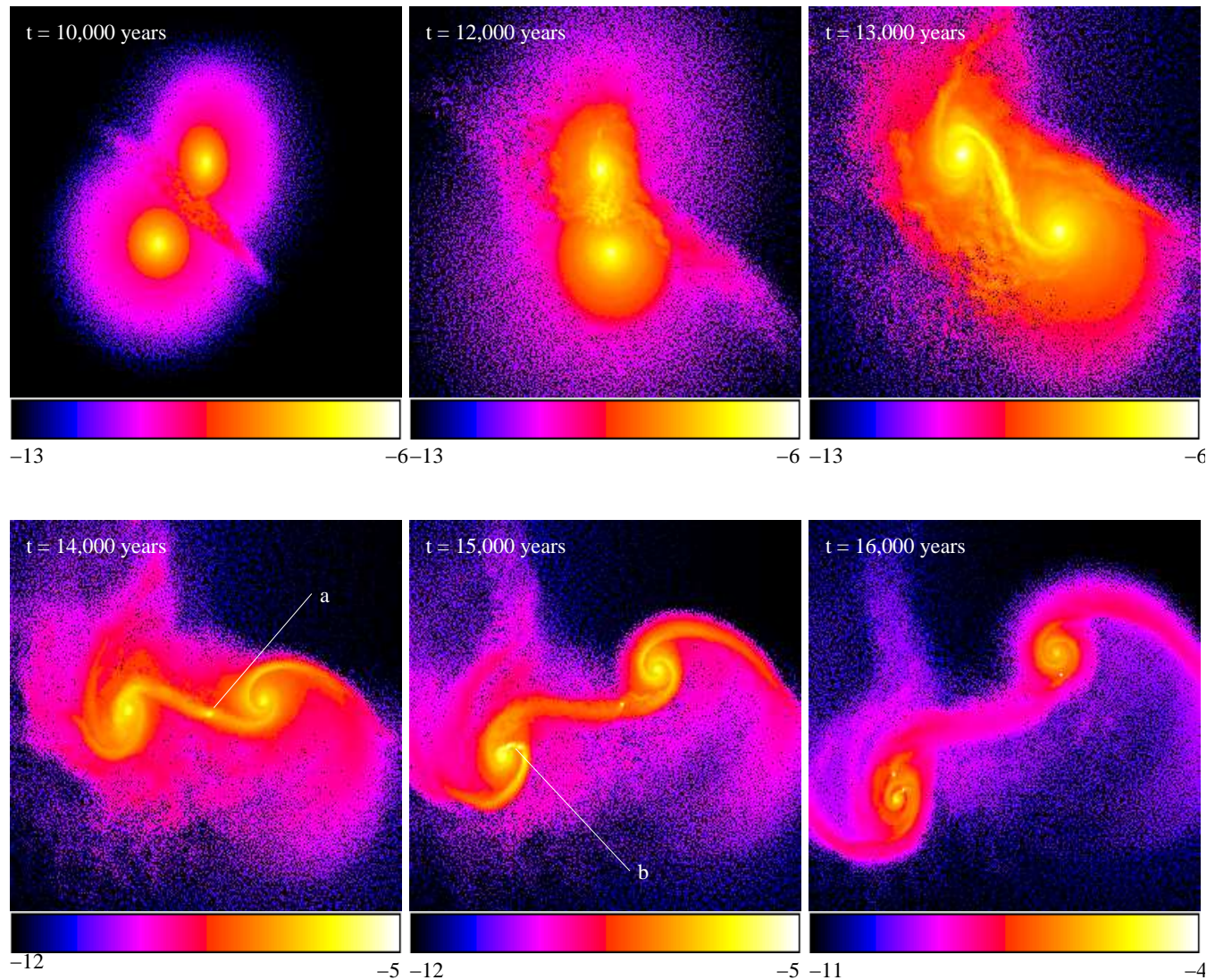


Figure 5. Snapshots of the prograde-prograde disk encounter “Conf3”. Time is indicated on the left top of each panel. The disks are counter-clockwise rotating in this view. The color bar under each panel gives the logarithm (based 10) of the density in units of M_{\odot}/AU^3 . Different density ranges are used to clearly show the clumps.

4.3 Varying Encounter Velocities

We investigated the effect of varying the relative velocity with two series of simulations, one containing non-coplanar encounters with both disks prograde, and one with coplanar encounters with two retrograde disks. In each series, the relative velocity of the encounters is repeated along with the number of object formed in Table 2.

With the exception of a special single case (“Vel_pro1”, see below), the number of clumps formed in an encounter generally decreases with increasing velocity. No clumps formed in prograde disks when the relative encounter velocity was above 4.0 km/s. This result can be qualitatively understood by comparing the interaction timescale with the dynamical timescale of the disks. Though gravitational interactions occur regardless whether or not there is a physical impact, these simulations indicate that significant changes in the density profile occur only when the disks are close enough to physically impact. The interaction timescale is

Table 2. Number of objects formed in the simulations with different encountering velocities

Case	Velocity (km/s)	Number of Clumps	Fragmentation Mechanism
Vel_pro1	0.8	1	Circumbinary disk
Vel_pro2	2.0	3	Tidal structure and disk
Vel_pro3	4.0	0	
Vel_pro4	6.0	0	
Vel_retro1	0.8	8	Shock layer and disk
Vel_retro2	2.0	2	Disk only
Vel_retro3	4.0	3	Disk only
Vel_retro4	6.0	1	

approximately,

$$t_{\text{int}} = \frac{d_{\text{eff}}}{v} \quad (2)$$

where d_{eff} is the twice the disk diameter (4000 AU in this

case), which gives the rough separation for physical impact. v is the relative velocity of the encounter. The dynamical timescale within each disk is a function of radius r , given by,

$$t_{\text{dyn}}(r) = \frac{2\pi r^{3/2}}{\sqrt{GM_*}} \quad (3)$$

where G is the gravitational constant and M_* is the mass of the star. The encounter timescales t_{int} were 2.4×10^4 , 9.5×10^3 , 4.7×10^3 and 3.1×10^3 years for relative speeds 0.8, 2.0, 4.0 and 6.0 km/s, respectively. The dynamical timescale t_{dyn} was about 1.1×10^4 years at 400 AU and 3.9×10^3 year at 200 AU. The implication is that there was insufficient time during fast encounters, where $t_{\text{int}} < t_{\text{dyn}}$ to apply the torque that transfers angular momentum to change the disk profiles and causes fragmentation. This is more restrictive for prograde disks where tidal structures form further out at distances similar to 400 AU.

4.4 Captures and the Formation of Binary Stellar Systems

In the case “Vel_{pro1}”, star capture occurred and the two encountering stars formed a binary system. Both disks were prograde and large tidal tail structures formed when the disks passed periastron. The tidal structure dissipated over time and carried away the excess angular momentum from the system, enhancing the formation of a close binary. The separation of the two components was about 90 AU, significantly smaller than the periastron of the trajectory (about 300 AU taking into account the effect of gravitational focusing). The circumbinary disk was about 500 AU in radius. At a later time it also fragmented to form a 20 Jupiter mass object.

Another case where stellar capture occurred is the case “Q3” (as described in Section 4.1). Since the starting disk Q parameter is 2.1, the circumbinary disk became hotter and less massive compared to the standard cases. No fragments formed at the end of the simulation. The initial disks are retrograde and the encounter did not induce tidal structures.

The two cases above are the only ones where stellar capture occurred. Note that both of them have rather conservative choices of encounter velocities (0.8 km/s), with which the system are marginally bound at the initial state.

5 PROPERTIES OF THE OBJECTS FORMED

Most of the encounters produced clumps with the exception of those with high relative velocities or very stable initial disks (e.g. $Q_{\text{min}} > 2.1$). As described in the last section, bound objects can form from fragmentation of shock layers, instabilities within a disk and in tidal structures. Since the timescale of disk encounters (about 10,000 years) is short and encounters may happen when there is still a lot of material obscuring the stars, encounters in progress are unlikely to be observed whereas the sub-stellar objects formed may persist indefinitely. Though these objects may evolve substantially from their time of formation, particularly in terms of luminosity, simulated clump properties such as mass, angular momentum and orbital kinematics can be directly compared with properties of observed objects. In

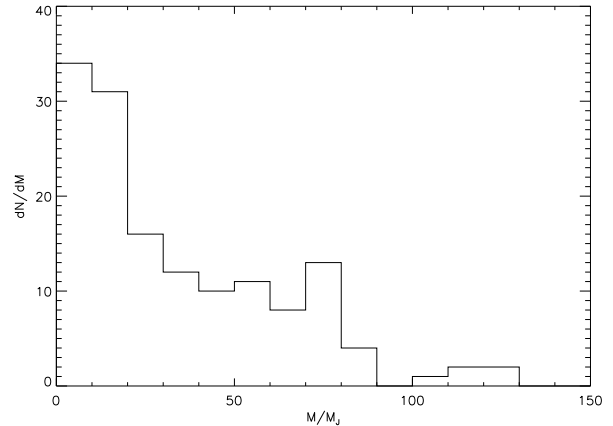


Figure 7. The mass distribution of 146 objects formed outside 50 AU in the 48 “Conf” simulations. The bin size is $5 M_J$.

the initial state, the disks were well resolved outside 50 AU. However, as the simulations progressed, additional matter accumulated in the inner disks improving the resolution elements per scale height. On the other hand, objects with 50 AU are likely to experience further evolution such as accretion and migration into the star. In addition, work by Rafikov (2007) has suggested that disks this close to a star are optically thick and unlikely to cool fast enough to fragment. For these reasons, we have excluded objects within 50 AU from the sample discussed below. However, the objects formed within 50 AU are not statistically different and properties such as the relative mass distribution would not be significantly altered if these objects were included. A total of 191 objects formed in our simulations (excluding the high Q cases) with 144 outside 50 AU.

5.1 Mass Distribution

The object masses range from 0.9 Jupiter masses (M_J) to $127 M_J$, extending into the stellar regime. The mass distribution is plotted in Figure 7. It was found that the number of objects generally decreases with increasing mass, consistent with the observed sub-stellar initial mass function (IMF). The simulated population does not include objects much below $10 M_J$). In this regime there are 1000 or fewer particles per object. The numerical gravitational softening (0.2 AU) could also inhibit the formation of smaller objects. Thus these simulations are unable to probe whether there is a physical mass cut-off in this range.

Observationally, the sub-stellar IMF in open clusters can be well described by a power-law $dN/dM \propto M^{-\alpha}$. For young open clusters such as Pleiades, λ Orionis and σ Orionis, the exponent α is close to 0.6 at low masses with an uncertainty of order 0.1 (Moraux et al. 2003; Barrado y Navascués et al. 2004; Caballero et al. 2007). An universal IMF was proposed by (Kroupa 2001) in which $\alpha = 0.3 \pm 0.7$ in the range $0.01M_{\odot} < M_* < 0.08M_{\odot}$. In this work, we fit the mass distribution of the sub-stellar region ($M < 0.08M_{\odot}$) and the best fit gives $\alpha = 0.6$ with χ^2 uncertainty 0.15 (Figure 8), consistent with the observed values. Above the stellar boundary the number of objects declines more rapidly with mass and a break is apparent

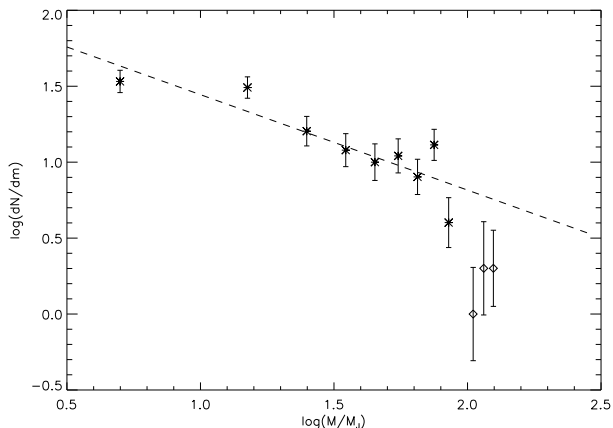


Figure 8. The logarithmic mass distribution of the objects. The error bars were calculated assuming Poisson errors $\propto \sqrt{N_{\text{bin}}}$. *Stars*: sub-stellar objects ($M \leq 80M_J$); *Diamonds*: low mass stars ($M > 80M_J$); *Dashed line*: linear fit of the logarithmic distribution of sub-stellar objects $dN/dM \propto M^{-\alpha}$, with $\alpha = 0.6$

near $0.08 M_{\odot}$ (or about 0.1 of the central mass) which is also consistent with the trend reported by (Kroupa 2001). There are only 9 objects in total that are beyond $0.08 M_{\odot}$ and thus the statistics are poor. More simulations, including those with varying central star masses, are required to explore the resulting mass function in the low mass, stellar regime.

5.2 Shapes and Angular Momenta

Most of resultant clumps in our simulation are not spherical but have highly flattened, disk-like shapes (height to radius ratio ~ 0.1), as shown in Figure 9. The radii of the disks range from 0.1 AU to 10.0 AU. The lower bound is likely to be associated with the resolution limit (0.2 AU). The disk-like shape is maintained by the high spin angular momentum of each clump. Depending on the mass and size, the total angular momenta of the clumps range from 10^{47} to 10^{51} g cm²/s. Assuming the total angular momentum is conserved during the evolution and adopting a typical radius of a brown dwarf to be 7.0×10^9 cm (Burrows et al. 1998), the rotation speed at the edge of the brown dwarf would be 10 times the break up speed. Thus the proto-brown dwarf disks must shed rotation in order to collapse down to a proto-BD. This result is consistent with recent mid-IR, sub-millimeter, and millimeter observations of the spectral energy distributions (SEDs) of young brown dwarfs, which indicate that most of them are surrounded by circumstellar disks (e.g., Muench et al. 2001). A T Tauri accretion phase has also been indicated in some young BD disks by the detection of broad, asymmetrical $H\alpha$ lines (Jayawardhana et al. 2003). The IR excess in SEDs was found to decrease as the age of BDs increases, which suggests that the BD disks evolve from flared to flat geometry similar to proto-stellar disks (Mohanty 2005). The clumps in our simulations are flat partly due to the assumed isothermal EOS. As explored in section 6, these dense condensations are probably optically thick and would thus be hotter and more puffed up in nature.

The simulations were terminated a few thousand years

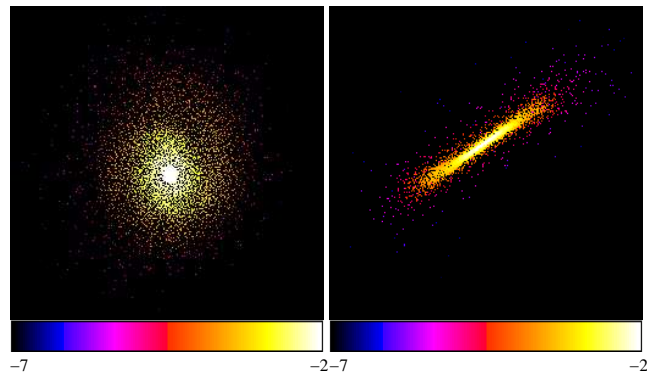


Figure 9. A resultant clump with typical disk-like shape. Both panels are 14 AU on a side. The clump has a disk radius of about 4 AU. *Left*: The object projected in the x-y plane; *Right*: The object projected in the x-z plane. The gray scale indicates the density in logarithmic space in code units M_{\odot}/AU^{-3} .

after the first object formed due to computer time limitations. In some objects, like the one shown in Figure 9, by the time the simulation was halted, the gas with lower specific angular momentum had started to condense into the center and a density gradient had also been established. Because the gravitational softening (0.2 AU) is comparable to the size of most clumps, our ability to resolve the structure and follow the evolution of the proto-BD disks is limited. However, it can be expected in later evolution a central proto-BD will form and the surrounding disk will accrete onto it on a viscous timescale.

In the majority of cases where clumps formed from fragmentation of disks, the spin directions of the proto-BD disks are similar to their parent proto-stellar disks. In the case where the shock layer fragments, however, the resultant proto-BD disk may spin in a direction different from both disks. For the proto-BD disks that are still orbiting the star, further interaction with their parent disk will influence the final spin.

5.3 Binary Brown Dwarfs and Multiple Systems

Typically where fragmentation occurred more than one object was produced. About 15 percent of the objects are in BD-BD binary systems. This fraction is consistent with the observed binary fraction (around 10 ± 10 % at the range 0.01 to $0.1 M_{\odot}$) (cf. Figure 3 Hubber & Whitworth 2005). In most cases, the binaries formed from secondary fragmentation of very large disk-like clumps. Further numerical studies with higher resolution are necessary to investigate this question in detail because, although the Jeans mass was well resolved before fragmentation and most of the clumps are resolved by at least 1000 particles, the Jeans masses of the clumps themselves decrease so quickly with increasing density that they are only marginally resolved in our simulations. Without resolving the Jeans mass, it has been suggested that fragmentation could be artificially enhanced (Bate & Burkert 1997). However, given the very high spin rate of the clumps, secondary fragmentation is likely to occur, according to Matsumoto & Hanawa (2003).

Most of the BD binary systems were still bound to the central stars when the simulations were terminated. For ex-

ample, in case “Conf5”, the binary system orbits the star at ~ 140 AU, with the two components (mass $19 M_J$ and $13 M_J$) orbiting each other in a period of around 30 years and with separation about 3 AU. Each component has a highly flattened shape. In future evolution, it is expected that some of these binaries will merge to the star, leave the system, or be ejected in close interactions with other objects. The surviving systems are likely to remain hierarchical star-BD multiples. Thus the collision mechanism may explain the origin of observed star-BD multiple systems such as GL 569, where a recently confirmed BD triple (GL 569B) orbits the primary, an M2.5V star (GL 569 A) (Gorlova et al. 2003; Simon et al. 2006). The system is about 100-125 Myrs old so no BD disks were observed. However, in younger BD multiples accretion signals have been detected (Kraus et al. 2006), indicating accretion disks surrounding components of the multiple.

5.4 Orbits and Further Evolution of the Resultant Clumps

Objects in our simulations typically formed at least 50 AU away from the closest star. Approximately 60 percent of the objects formed were not bound to the system. The percentage is higher for coplanar encounters, in which the shock layer fragmentation can take place relatively far out in the gravitational potential of the stars. The unbound objects may leave the whole system to become free floating BDs (or BD binaries) or low mass stars. For the objects that are bound to the star, the orbital properties vary from case to case. About 5 percent of the orbits have very large semi-major axes (> 500 AU) but are still bound to the system. Since the outer proto-stellar disk was dispersing in most encounters, sub-stellar objects in large orbits were unlikely to accrete additional gas to become low mass stars. Hence these objects may remain as wide-separation BD companions, which have been detected in observations (Gizis et al. 2001). Where more than one object orbits the star on nearby orbits dynamical interactions can take place resulting in the preferential ejection of lower mass objects (Reipurth & Clarke 2001). The 11 objects that were ejected to significant distances during the simulations were lower in mass. However, the majority of the objects were unbound and would ultimately become free-floating.

For the clumps that stay in the dense region of the proto-stellar disks (within 100 AU), the future growth and evolution depend on the rate that the gas accretes onto the objects. Under the assumption of efficient gas accretion, as in the competitive accretion scenario (Reipurth & Clarke 2001; Bate et al. 2003), these objects may eventually become low-mass stars over timescales much longer than those simulated here.

6 COOLING APPROXIMATIONS

6.1 Optically Thick Approximation

The simulated disks produced dense regions as they evolved and reached the point where they were no longer uniformly optically thin. The disk material itself tended to remain optically thin ($\tau < 1$) and was thus capable of efficient cooling

but the fragments within the disk reached high densities where the radiative cooling times became very long. Thus on the timescale of these simulations, the interiors of the fragments were effectively adiabatic.

In earlier work on proto-planetary disk fragmentation (Mayer et al. 2004), the approximation of converting the entire simulation to adiabatic gas was employed to test the behaviour in this regime. This corresponds to the extreme where cooling is completely absent. A less extreme test with strong suppressed cooling is to smoothly interpolate from efficient black-body cooling when the gas is optically thin to no cooling in the optically thick regime. Optically thin black-body radiative losses are given by,

$$L = 4\kappa\sigma T^4 M \quad (4)$$

where L is the luminosity, κ is the opacity, T is the temperature and M is the total mass. The opacity was taken to be $1 \text{ cm}^2 \text{ g}^{-1}$ at $T = 60\text{K}$ with a power-law variation with temperature as $T^{1.3}$. This is consistent with the dust opacity values calculated by d’Alessio et al., as tabulated in Mejia (2004), over the range of 10-300 K.

We then took a late stage of a representative run “Conf30” at 15000 years, after fragmentation had occurred, and measured the optical depth to infinity in 12 directions (corresponding the faces of a dodecahedron) for each particle. This allowed us to estimate the averaged effective optical depth, $\tau_{\text{eff}} = -\log_e \int_{\Omega} e^{-\tau(\Omega)} d\Omega/4\pi$. We found that the effective optical depth correlates fairly well with gas density in the regime, $\rho = 10^{-16}$ to $10^{-12} \text{ g cm}^{-3}$, where the material transitions from optically thin to ($\tau_{\text{eff}} \sim 0.1$) to optically thick ($\tau_{\text{eff}} \sim 10$) as $\tau_{\text{eff}} = 10^{8.1+0.56\rho}$. The *rms* deviation of the fit is 0.16 dec in τ . Assuming isotropic emission, we can then estimate the fraction of the emitted light (given by equation 4) that escapes the disk entirely. We then assume that the rest of the emission is absorbed on-the-spot, an approximation commonly used for optically thick lines in models of emission nebulae, so that the net radiative loss, L_p , from one particle is $L_p = 4\kappa\sigma T_p^4 m_p e^{-\tau_{\text{eff}}(\rho_p)}$, where m_p , T_p and ρ_p are the particle mass, temperature and density, respectively. In the limit of infinitesimal particle masses, this expression is proportional to the contribution to the surface flux from a mass of gas, $dm = \rho dl dA = d\tau/\kappa dA$. In the case of an infinite plane-parallel slab, when an analytic expression for τ_{eff} is used and the flux contribution is integrated from the surface to high optical depth the total surface flux asymptotically approaches the value of σT_p^4 .

The assumption for the main set of simulations was that the disk temperatures were set by heating from the central star offset by radiative losses so that the net temperatures were a function of the distance to the nearest star. To include the effect of heating by the star, the governing equation of the particle energy per unit mass, E_p , is,

$$\frac{dE_p}{dt} = 4\kappa\sigma e^{-\tau_{\text{eff}}(\rho_p)} (T(r_{\text{star}})^4 - T_p^4) - \frac{P}{\rho} \nabla \cdot \mathbf{v}|_p + \Lambda_{\text{shock},p}, \quad (5)$$

where $T(r_{\text{star}})$ is the temperature determined from an equilibrium between stellar heating and radiative losses at the radius r_{star} from the nearest star, $-\frac{P}{\rho} \nabla \cdot \mathbf{v}$ is the compressive heating term and Λ_{shock} is the shock heating term. Thus the model now includes compressive heating and shock heating. Outside the intense collision environment, where these process are unimportant in relation to stellar heat-

ing, the disk temperatures relax to the temperature as a function of radius assumed in the preceding sections. Overall, this is similar to the approximation employed by Stamatellos & Whitworth (2009), where local cooling was based on the amount of radiation escaping from regions with similar physical conditions in spherical collapse models. In the approximation used here the radiative loss rates were calibrated from similar disk cases.

Our approximation retains thermal energy indefinitely in the denser gas and is thus conservative with regard to ensuring that the fragmentation is not a result of favourable cooling assumptions. Detailed radiative transfer calculations should give results between this approximation and the isothermal EOS. It has been argued by Rafikov (2007) that the optically thick parts of proto-stellar disks are likely to be convective, in which case our neglect of radiation as a heat transport mechanism may not have a large impact on the disk structure. However, the cooling of the optically thin surface layers are approximately correct in this model. Full radiative transfer has been implemented within the Gasoline code (Rogers, Shen & Wadsley, *in preparation*) and will be applied to proto-stellar disk collisions as part of future work.

6.2 The Optically Thick Run

We re-ran the simulation we used to calibrate the effective optical depth-density relationship using the new cooling approximation. Figure 10 compares the disks at 14,000 years in the locally isothermal run (Panels that are labeled with “ISO_1” and “ISO_2”) with the ones in the new run (Panels labeled with “THICK_1” and “THICK_2”). Using the isothermal equation of state, one of the disks fragmented and formed ten bound objects, including two binary systems. However, when using the optical thick approximation, the cooling is suppressed and the disk does not fragment immediately. Instead, it is the tidal structure induced by the gravitational resonance that condensed and formed a clump at about 410 AU from the star. At later time steps, the gas in the tidal tail dissipated and the objects orbit the star at about 350 AU. The clump had a mass of $0.075 M_{\odot}$, close to the hydrogen burning limit.

Compared to the objects that formed in the corresponding isothermal run, the clump had a more spherical shape. Nevertheless, the angular momentum of the object was still very high, about 7.5×10^{50} g cm²/s. By the end of the simulation we did not see flattening as the clump could not cool with this approximation. If no angular momentum was lost the final object would spin at 30 times the break up speed. Hence we expect the clump to collapse to a disk similar to the ones formed in the isothermal run and that jets and fragmentation could occur in nature as before.

Thus with heavy cooling suppression, beyond that expected in nature, we retain our main result, i.e. there was still gas condensation and the formation of clumps due to encounters. The number and the shape of the clumps at the end of simulation was strongly affected. Exploring the effect of differing thermal regulation on encounter-induced fragmentation will be a target for future work.

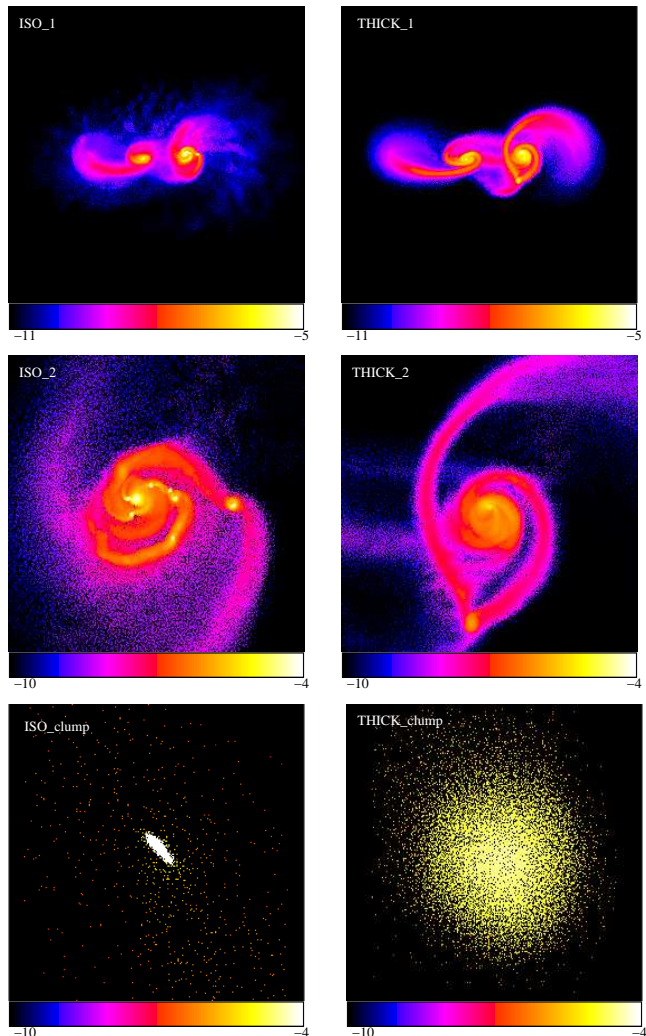


Figure 10. A $Q = 1.6$ disk encounter with isothermal EOS vs. our optical thick approximation. *Left:* The run with isothermal EOS (top and middle panels) and the typical shape of a clump (bottom panel); *Right:* The simulation that used optical thick approximation. The grey scale under each panel gives the density ranges in units of M_{\odot}/AU^3 .

7 DISCUSSION AND SUMMARY

In this work, the possibility of encounter-induced disk fragmentation as a mechanism for forming sub-stellar objects was investigated. The significant increase in resolution over previous work and the use of a realistic initial disk model ensures that the initial fragmentation to form clumps was physically modeled within the constraints of our thermal regulation assumptions. These simulations have shown that encounters can trigger the formation of brown dwarfs as well as low mass stars.

We found that strong instabilities can be triggered in stable disks with initial $Q_{\min} < 2.1$, by lowering the local Q value with large gas inflows during an encounter. A relatively steep surface density profile ($\Sigma \propto r^{-3/2}$) and a relative high ambient temperature (40 K) were used in our simulations. If disks have shallower density profiles, as was found in some observations of early disks (Andre et al. 2000), and hence

have large portions of their mass in the cooler, outer region, the rate of fragmentation could be even higher.

By studying collisions with random initial orientations, it was also found that retrograde encounters (disks with retrograde spins relative to the orbital angular momentum) more effectively transport angular momentum, triggers gas inflows and ultimately produce more clumps on average than the prograde ones (Figure 6). These results differs from those reported for simulations of star-disk encounters which indicated that prograde encounters were more efficient in triggering disk instability (e.g. Boffin et al. 1998; Lodato et al. 2007). The difference may relate to having an extended perturber.

Dense shock layers may occur during coplanar encounters and result in objects as seen in previous work. However, our results indicate that only slow coplanar encounters (cases “Conf1” and “Conf2”), where the shock layer had time to accrete substantial mass, can undergo fragmentation. This differs from the results of Watkins et al. (1998b), where a large fraction of their objects formed in the fragmentation of shock layers in both coplanar and non-coplanar cases. This discrepancy may be due to the use of more unstable initial disks, numerical problems related to lower resolution or the absence of vertical structure in the disk models (Appendix A). However it should be noted that coplanar encounters are very rare if the disk orientations are random.

The velocity constraint found in our simulations implies the number of BDs produced in encounters is a strong function of the velocity dispersion in the young star cluster. However, the numerical trend as a function of cluster density can be complicated. On one hand, more massive and denser clusters usually have larger velocity dispersions and hence likely to produce fewer sub-stellar objects per encounter. On the other hand, high number density will increase the encounter rate which could potentially increase the BD numbers.

The encounter mechanism is complementary to other mechanisms for producing BDs. Proto-stellar disks in close proximity are naturally produced when star cluster formation is simulated from cloud collapse. Simulations of massive clouds typically lack the resolution necessary to form large stable disks or to follow subsequent encounters in detail (Bate et al. 2003). Thus this mechanism is compatible with ideas such as competitive accretion and turbulent fragmentation. The relative importance of these processes for forming proto-stars may influence the typical separation and orientation of proto-stellar disks and thus affect the starting point for encounter driven object formation. These statistics also depend the larger environment, such as the size, the mass and the amount of turbulent motion in the star forming cloud.

A dynamical encounter origin for some BDs might explain observed differences in binary statistics between stars and BDs in different cluster environments. Some observations have indicated that the ratio of BDs to stars is higher in denser clusters. For example, Slesnick et al. (2004) found in Trapezium, the number ratio (R_{ss}) of sub-stellar objects ($0.02 \leq M/M_{\odot} \leq 0.08$) over stars ($0.08 < M/M_{\odot} < 10$) is about 0.20, while Luhman et al. (2003) calculated for Taurus aggregates and IC 348 R_{ss} is about 0.14 and 0.12 respectively, significantly lower than Trapezium. The results are not conclusive as other surveys have indicated that R_{ss} in

Taurus is comparable with that in Trapezium (Levine et al. 2006, and references therein). To make further predictions about how the BD ratio may be related to the cluster properties, more comprehensive simulations and parameter studies would be required, in which the encounter rate in different cluster environment is estimated in detail and the encounter velocity parameter space is well sampled.

Almost all the clumps formed in the isothermal simulations have flattened shapes. In the future evolution, we expect these clumps to centrally condense to form a proto-BD with a disk. Material should accrete onto the central object on the viscous timescale. Observations indicate that the accretion rate for low mass stars and sub-stellar objects can be approximately fitted by $\dot{M} \sim 10^{-8} M_{\odot} \text{ yr}^{-1} (M/M_{\odot})^2$ (Muzerolle et al. 2003). Hence for a relatively massive brown dwarf with $0.05 M_{\odot}$ the accretion rate is around $2.5 \times 10^{-11} M_{\odot} \text{ yr}^{-1}$. With this rate the BD disk can have a mass as low as $10^{-4} M_{\odot}$ and still have lifetime comparable to proto-stellar disks. To shed angular momentum, a proto-BD disk might also launch bipolar outflows or form sub-stellar companions. Since most BDs formed during encounter-induced disk fragmentation have large excess angular momenta, we expect outflows or companions to be common for young BD formed this way. Recent observations have found forbidden emission lines in BD spectra, suggesting outflows (Natta et al. 2004). In particular, an outflow from a young BDs ρ Oph 102 has been spatially resolved (Whelan et al. 2005). Some of proto-BD disks in our simulations underwent secondary fragmentation and form binary BD systems (cf. Section 5.3). Due to resolution and physical limitations, this result needs to be confirmed with better simulations. However, the rapid rotation of these disk favours fragmentation (Matsumoto & Hanawa 2003) which can form companions of a range of masses. This provides a mechanism for forming the observed BD-BD binaries with the small separations peaking at ~ 1 to 4 AU and with almost equal mass components (Whitworth et al. 2007, and references therein). Planetary-mass companions have also been observed surrounding young BD (e.g. 2M1207b Chauvin et al. 2005).

Possible future work could follow several directions. Firstly, the predictive power would be improved if parameters other than disk configuration were to be well sampled, particularly the velocity of the encounter, the disk properties and the star masses. Combined with a detailed calculation of encounter rates as a function of cluster density and velocity dispersion, quantitative results could be obtained to directly compare with the observations of BD to star ratios, R_{ss} . Secondly, when the optical-thin approximation fails in high density regions, the effects of shock heating and radiative cooling become more important and should be further investigated. Including radiative transfer in the simulation is likely to reduce the number of objects formed per encounter, and provide for more realistic evolution of the proto-BD disks (as indicated in the optically thick approximation, section 6). Alternately, with simplified models, the evolution of the clump themselves could be followed over long timescales.

APPENDIX A: RESOLUTION REQUIREMENTS

When designing the simulation the resolution requirement was estimated from the Bate & Burkert (1997) criterion, i.e., the Jeans mass should be resolved by at least twice the number of neighbour particles, $N_{Neighbor}$. In our simulations we used exactly 32 neighbours. In the initial condition, the density of our disk varies from $10^{-13} g/cm^3$ to $10^{-20} g/cm^3$. Using our temperature profile, described in section 2, the Jeans mass at the highest density for the initial disk was estimated to be $0.0095 M_{\odot}$. Hence resolving the initial disk of $0.6 M_{\odot}$, which contains about 63 of these smallest Jeans masses requires about 4000 particles for each disk. During the encounter, however, as shown in Section 4, large inflows of gas and unstable modes increase the density significantly. The density typically increases by three orders of magnitude locally where fragmentation will then occur. Therefore to resolve the smallest Jeans mass during the simulation significantly more particles were necessary. To correctly simulate gas with densities up to $10^{-10} g/cm^3$ about 127000 particles were needed. We used 200000 particles for each disk, which met the above requirement and ensured that the fragmentation was physically modeled.

The effects of resolution and the finite scale height were studied with two-dimensional simulations and through analytical arguments by Nelson (2006). We performed two sets of comparison simulations to investigate these effects in three dimensions. The first set consisted of three simulations of isolated disks with the same surface density and temperature profile and a minimum Toomre Q of 1.3, well above the critical value of 0.8. The first disk was modeled by the single layer of 2000 particles. The second had 20000 particles but still had no vertical structure. The third one used 200000 particles and the vertical structure was modeled using the methods described in section 2. Figure A1 depicts the results for each disk at a later time step.

While no structure formed in the third, well-resolved simulation, strong gravitational instabilities and fragmentation occurred in the first two within several outer orbital periods. Note that in the first case with 2000 particles the Jeans mass was not resolved in the high density region of the initial disk. For the second case although the Jeans mass was fully resolved everywhere in the initial condition (not necessary during the simulation), the lack of vertical structure in the model was still destabilizing and artificial fragmentation occurred. Although it is not clear from these two simulations which factor (resolving Jeans mass or modeling the finite thickness) is more important to prevent unphysical fragmentation, the test simulations show that it is essential to consider both factors in the simulation.

The second series consist of two simulations of retrograde dynamical encounters of disks with $Q = 2.1$. The disks were very stable in isolated runs. The dynamical parameters of the encounter was the same as case “Q3” in Table 1. In the first simulation the disks were modeled by single layer of 2000 particles, while in the second the disk was resolved by 200000 particles and had vertical structures. The results is depicted in Figure A2.

Similar to the isolated runs, without properly resolving the Jeans mass and scale height, the encounter triggered fragmentation at time step of 19700 years in the shock layer

between two coplanar disks (Panel 2, Figure A2). In the second simulation, although the shock layer was still produced (Panel 4), no fragmentation occurred in the layer. The encounter was also modeled using 400000 particles with the same result.

In summary, regardless of whether the disks are passively evolving or undergo a physical impact, numerical effects may be significant if the Jeans mass is not resolved or if no vertical structure is presented in the disk model. The major numerical effect is then enhanced instability and the formation of artificial clumps. Our resolution of 200000 particles was chosen based on a conservative estimate of resolution requirements, e.g., it assumed the density of the whole disk could increase up to $10^{-10} g/cm^3$. In fact, most outer region of the disk had density below $10^{-12} g/cm^3$ when fragmentation initial occurred. With this resolution it was ensured that the initial disk fragmentation (if any) was physical. We also performed simulations at higher resolution (400000 and 800000 particles) for some specific cases and the results converged.

REFERENCES

- Andre, P., Ward-Thompson, D., & Barsony, M. 2000, *Protostars and Planets IV*, 59
- Barrado y Navascués, D., Stauffer, J. R., Bouvier, J., Jayawardhana, R., & Cuillandre, J.-C. 2004, *ApJ*, 610, 1064
- Bate, M. R., & Burkert, A. 1997, *MNRAS*, 288, 1060
- Bate, M. R., Bonnell, I. A., & Bromm, V. 2002, *MNRAS*, 332, L65
- Bate, M. R., Bonnell, I. A., & Bromm, V. 2003, *MNRAS*, 339, 577
- Boffin, H. M. J., Watkins, S. J., Bhattal, A. S., Francis, N., & Whitworth, A. P. 1998, *MNRAS*, 300, 1189
- Boss, A. P. 2001, *ApJ*, 563, 367
- Briceño, C., Luhman, K. L., Hartmann, L., Stauffer, J. R., & Kirkpatrick, J. D. 2002, *ApJ*, 580, 317
- Burrows, A., et al. 1998, *Brown Dwarfs and Extrasolar Planets*, 134, 354
- Caballero, J., Bjar, V., Rebolo, R., Eisloffel, J., Zapatero Osorio, M., Mundt, R., Barrado Y Navascus, D., Bihain, G., Bailer-Jones, C., Forveille, T., Martn, E. 2007, *A&A*, 47[0], 903
- Chabrier, G. 2002, *ApJ*, 567, 304
- Chauvin, G., Lagrange, A.-M., Dumas, C., Zuckerman, B., Mouillet, D., Song, I., Beuzit, J.-L., & Lowrance, P. 2005, *A&A*, 438, L25
- Chiang, E. I., & Goldreich, P. 1997, *ApJ*, 490, 368
- D’Alessio, P., Calvet, N., & Hartmann, L. 2001, *ApJ*, 553, 321
- Elmegreen, B. G. 1999, *ApJ*, 522, 915
- Gammie, C. F. 2001, *ApJ*, 553, 174
- Gauvin, L. S., & Strom, K. M. 1992, *ApJ*, 385, 217
- Gizis, J. E., Kirkpatrick, J. D., Burgasser, A., Reid, I. N., Monet, D. G., Liebert, J., & Wilson, J. C. 2001, *ApJL*, 551, L163
- Gorlova, N. I., Meyer, M. R., Rieke, G. H., & Liebert, J. 2003, *ApJ*, 593, 1074
- Guieu, S., Dougados, C., Monin, J.-L., Magnier, E., & Martín, E. L. 2006, *A&A*, 446, 485

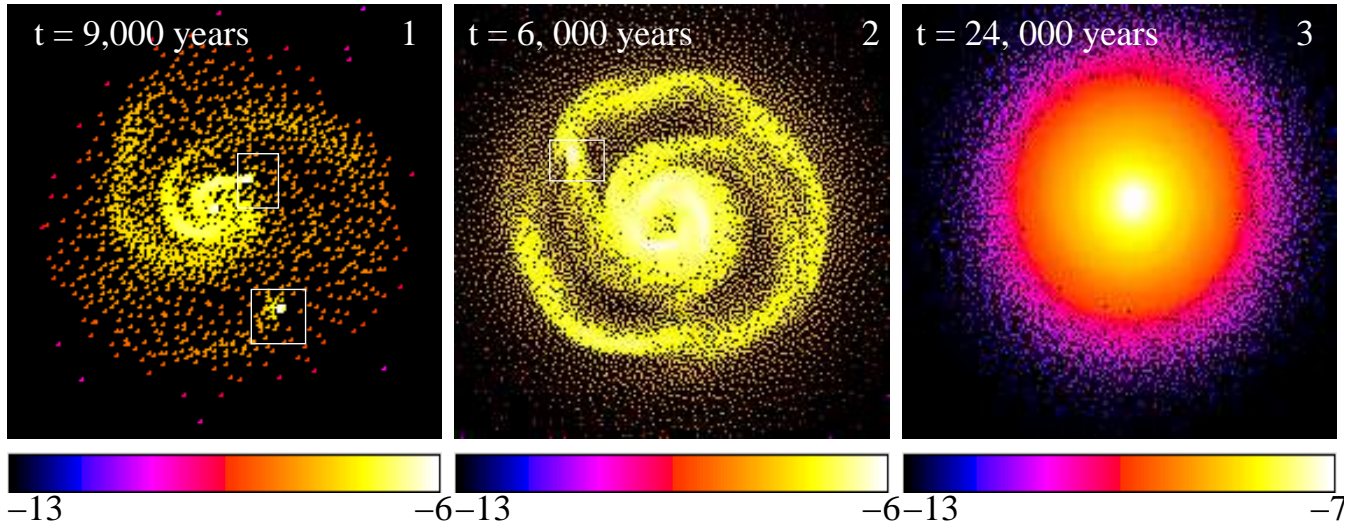


Figure A1. Isolated disk simulations with different resolutions and disk models. All three disks have $Q = 1.3$ initially. Time steps for each snapshot are given in the upper left corners. Boxed regions indicate the fragments (if any). The grey scale under each panel gives the density ranges in units of M_{\odot}/AU^3 .

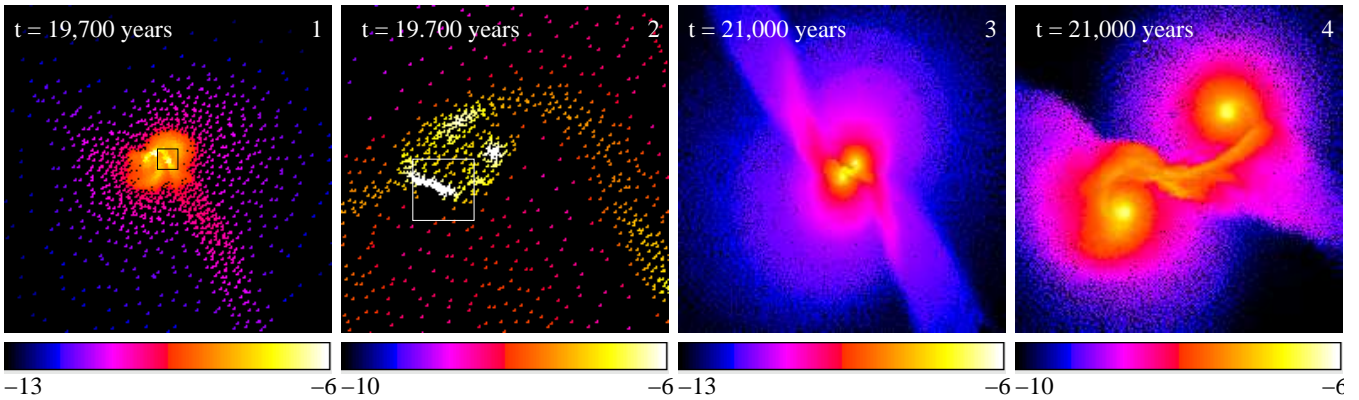


Figure A2. Disk encounter simulations with different resolutions and disk models. The disks have $Q = 2.1$ initially. Time steps for each snapshot are given in the upper left corners. The first two panels (panel 1-2) depicted the low resolution run and panel 3-4 are from the higher resolution one. Boxed regions indicate the fragments (if any). The grey scale under each panel gives the density ranges in units of M_{\odot}/AU^3 .

Hubber, D. A., & Whitworth, A. P. 2005, *A&A*, 437, 113
 Jayawardhana, R., Mohanty, S., & Basri, G. 2003, *ApJ*, 592, 282

Johnson, B. M., & Gammie, C. F. 2003, *ApJ*, 597, 131

Kim, W.-T., Ostriker, E. C., & Stone, J. M. 2002, *ApJ*, 581, 1080

Kraus, A. L., White, R. J., & Hillenbrand, L. A. 2006, *ApJ*, 649, 306

Kroupa, P. 2001, *MNRAS*, 322, 231

Krumholz, M. R., McKee, C. F., & Klein, R. I. 2005, *Nature*, 438, 332

Levine, J. L., Steinbauer, A., Elston, R. J., & Lada, E. A. 2006, *ApJ*, 646, 1215

Lin, D. N. C., Laughlin, G., Bodenheimer, P., & Rozyczka, M. 1998, *Science*, 281, 2025

Lodato, G., Meru, F., Clarke, C. J., & Rice, W. K. M. 2007, *MNRAS*, 374, 590

Luhman, K. L. 2000, *ApJ*, 544, 1044

Luhman, K. L., Stauffer, J. R., Muench, A. A., Rieke,

G. H., Lada, E. A., Bouvier, J., & Lada, C. J. 2003, *ApJ*, 593, 1093

Martín, E. L., Dougados, C., Magnier, E., Ménard, F., Magazzù, A., Cuillandre, J.-C., & Delfosse, X. 2001, *ApJ*, 561, L195

Matsumoto, T., & Hanawa, T. 2003, *ApJ*, 595, 913

Marcy, G. W., & Butler, R. P. 2000, *PASP*, 112, 137

Mayer, L., Quinn, T., Wadsley, J., & Stadel, J. 2004, *ApJ*, 609, 1045

Mejia, A. C. 2004, Ph.D. Thesis,

Mohanty, S. 2005, *Protostars and Planets V*, 8532

Morau, E., Bouvier, J., Stauffer, J. R., & Cuillandre, J.-C. 2003, *A&A*, 400, 891

Muench, A. A., Alves, J., Lada, C. J., & Lada, E. A. 2001, *ApJL*, 558, L51

Mundy, L. G., Looney, L. W., & Welch, W. J. 2000, *Protostars and Planets IV*, 355

Muzerolle, J., Hillenbrand, L., Calvet, N., Briceño, C., & Hartmann, L. 2003, *ApJ*, 592, 266

- Natta, A., Testi, L., Muzerolle, J., Randich, S., Comerón, F., & Persi, P. 2004, *A&A*, 424, 603
- Nelson, A. F., 2006, *MNRAS*, 373, 1039
- Padoan, P., & Nordlund, Å. 2004, *ApJ*, 617, 559
- Pickett, B. K., Mejía, A. C., Durisen, R. H., Cassen, P. M., Berry, D. K., & Link, R. P. 2003, *ApJ*, 590, 1060
- Price, D. J. & Bate, M. R. 2009, *MNRAS*, *accepted*
- Rafikov, R. R. 2007, *ApJ*, 662, 642
- Reipurth, B., & Clarke, C. 2001, *AJ*, 122, 432
- Rice, W. K. M., Lodato, G., & Armitage, P. J. 2005, *MNRAS*, 364, L56
- Simon, M., Bender, C., & Prato, L. 2006, *ApJ*, 644, 1183
- Slesnick, C. L., Hillenbrand, L. A., & Carpenter, J. M. 2004, *ApJ*, 610, 1045
- Stamatellos, D. & Whitworth, A. P. 2009, *MNRAS*, 392, 413
- Thies, I., Kroupa, P., & Theis, C. 2005, *MNRAS*, 364, 961
- Toomre, A. 1964, *ApJ*, 139, 1217
- Toomre, A., & Toomre, J. 1972, *ApJ*, 178, 623
- Truelove, J. K., Klein, R. I., McKee, C. F., Holliman, J. H., II, Howell, L. H., & Greenough, J. A. 1997, *ApJL*, 489, L179
- Wadsley, J. W., Stadel, J., & Quinn, T. 2004, *New Astronomy*, 9, 137
- Watkins, S. J., Bhattal, A. S., Boffin, H. M. J., Francis, N., & Whitworth, A. P. 1998, *MNRAS*, 300, 1205
- Watkins, S. J., Bhattal, A. S., Boffin, H. M. J., Francis, N., & Whitworth, A. P. 1998, *MNRAS*, 300, 1214
- Whelan, E. T., Ray, T. P., Bacciotti, F., Natta, A., Testi, L., & Randich, S. 2005, *Nature*, 435, 652
- White, R. J., Greene, T. P., Doppmann, G. W., Covey, K. R., & Hillenbrand, L. A. 2007, *Protostars and Planets V*, 117
- Whitworth, A., Bate, M. R., Nordlund, Å., Reipurth, B., & Zinnecker, H. 2007, *Protostars and Planets V*, 459
- Yorke, H. W., & Bodenheimer, P. 1999, *ApJ*, 525, 330
- Vorobyov, E. & Basu, S., 2009, *MNRAS*, 393, 822